Systematic comparison of 1D and 2D hydrodynamic models for the assessment of hydropeaking alterations

Matthias Bürgler[a,*], David F. Vetsch[a], Robert M. Boes[a], Davide Vanzo[a]

[a]*Laboratory of Hydraulics, Hydrology and Glaciology, ETH Zurich, Switzerland.*

Abstract

Numerical hydrodynamic models enable the simulation of hydraulic conditions under various scenarios and are thus suitable tools for hydropeaking related assessments. However, the choice of the necessary model complexity and the consequences of modelling choices are not trivial and only few guidelines exist. In this study we systematically evaluate numerical one-dimensional (1D) and two-dimensional (2D) hydrodynamic models with varying spatial resolution regarding their suitability as input for hydropeaking-sensitive, ecologically relevant hydraulic parameters (ERHPs), and their computational efficiency. The considered ERHPs include the vertical dewatering velocity, the wetted area variation between base and peak flow and the bed shear stress as a proxy for macroinvertebrate drift. We then also quantified the habitat suitability of brown trout for different life stages. The evaluation is conducted for three channel planforms with morphological characteristics representative for regulated Alpine rivers, ranging from alternating bars to a braiding river morphology. Our results suggest, that while a highly resolved 1D model is sufficient for accurate predictions of the dewatering velocity and wetted area in the less complex alternating bar morphology, a 2D model is recommended for more complex wandering or braiding morphologies. For the prediction of habitat suitability and bed shear stress, a 1D model appears to be always insufficient, and a highly resolved 2D model is suggested. Reducing the spatial resolution of 2D models leads to computational efficiency similar to 1D, while providing more accurate results. This study can serve as guideline for researchers and practitioners in the selection and setup of hydrodynamic models for hydropeaking.

Keywords: Hydropeaking, Hydrodynamic modelling, River morphology, Computational efficiency, 1D-2D comparison,

1. Introduction

Electricity generation by high-head hydropower plants (hereinafter HPP) plays a key role in responding to short term fluctuations in the electricity demand. The call for renewable and carbon-neutral energy

*corresponding author: buergler@vaw.baug.ethz.ch

sources likely increases the intermittent electricity production by solar or wind energy in the future, further underpinning the important role of HPP in balancing electricity supply and demand [29, 22].

However, the storage of water and partly sediment in high-head reservoirs for electricity generation alters the downstream flow regime, sediment transport and river morphology [7, 35]. Furthermore, hydropeaking introduces unnatural flow variations in downstream river sections and has been be associated with changes of the ecohydraulic regime, with severe impacts on the abundance and composition of the local flora and fauna [3, 30, 45], as well as on their habitat [5, 43]. Drift of individual species due to a sudden increase in discharge has been shown to have adverse effects on the population size of macroinvertebrates [10, 34] and fish [1].

Different studies indicate a displacement of suitable habitat between base and peak flows and a reduction of persistently available habitat due to frequent variations in flow depths and velocities [5, 43], with severe impacts on populations of immobile species or life stages with low mobility. Sudden decreases in discharge related to hydropeaking has been reported to result in mortality of fish [21, 37, 49], fish eggs [12] and macroinvertebrates [36] due to stranding.

The magnitude of hydropeaking alterations relates also with river morphology. More heterogeneous river morphologies might reduce adverse impacts of hydropeaking due to increased availability of shelter (refugia) during peak flows [43, 52]. However, also the stranding risk of fish is found to increase in more complex and heterogeneous morphologies, as a result of direct stranding on gravel banks or trapping inside channels or potholes [49, 31].

Legislation such as the Water Framework Directive (WFD) in the European Union or the Federal Act on the Protection of Waters in Switzerland request the mitigation of adverse effects on waterbodies from hydropeaking. In literature, three types of mitigation measures are identified [9, 28, 43]: (i) Operational measures, such as reducing the discharge ratio between peak and base flow or the vertical dewatering velocity; (ii) constructional measures such as building compensation basins and (iii) restoration measures to improve the overall ecological conditions in river reaches affected by hydropeaking. The efficient design of such mitigation measures often requires the assessment of ecological impacts from hydropeaking under status quo, as well as under different mitigation scenarios.

Numerical hydrodynamic models facilitate predictions of the hydro-morphological state of a river reach under different discharge scenarios. Simulated spatial distribution of flow velocity and depth can be used for the calculation of Ecologically Relevant Hydraulic Parameters (ERHPs) [sensu Vanzo et al. [52]], and habitat quantity and quality. Such metrics are proxies for more complex ecological impacts and are useful to evaluate the effectiveness of potential mitigation scenarios. Examples of ERHPs in literature are the dewatering velocity or the percentage of wetted area variation between peak and base flow [e.g. 47].

A consequence of the application of numerical models to generate primary input data is that model accuracy affects the quantification of the considered ecologically relevant metrics. Accuracy primarily depends on the choice of mathematical equations and on the spatial discretization of such equations. Despite increasing availability of computational resources and progress in numerical solutions [46, 51], computational costs for multi-dimensional models of river sections are not negligible [16]. Eventually, the choice of appropriate model complexity is a trade-off between prediction accuracy and computational cost.

Various studies apply numerical hydrodynamic models for hydropeaking impact analysis and environmental assessment. For example, Person [43] and Boavida et al. [5] make use of a two-dimensional (2D) hydrodynamic model in combination with the habitat model CASiMiR [38] for habitat modelling of fish. Quantity, quality and location of different fish habitats were computed with a cross sections based, pseudo 2D model, and compared to field measurements in García et al. [14]. Pasternack et al. [42] applied a 2D hydrodynamic model to evaluate different alternatives of spawning gravel replenishment using habitat and sediment entrainment criteria. Vanzo et al. [52] analysed the interactions between hydropeaking and river morphology for several ERHPs by employing a 2D model. Similarly, Hauer et al. [24] applied a one-dimensional (1D) hydrodynamic numerical model to investigate the influence of highly unsteady flow conditions resulting from hydropeaking on river morphology, while Hauer et al. [23] investigated streamwise changes in the vertical dewatering velocity using a 1D and a 2D model. Tuhtan et al. [49] investigated the stranding risk of fish related to hydropeaking under consideration of different river morphologies, also using a 2D model.

Few studies address the accuracy of applied models with regard to model dimensionality or provide recommendations on the necessary spatial resolution. Casas-Mulet et al. [12] evaluated the performance of a 1D model for the calculation of stranding areas by comparing simulated and measured inundation area. A similar approach was followed in Juárez et al. [28] for a 2D hydrodynamic model. Brown and Pasternack [8] compared 1D and 2D numerical models for the prediction of hydraulic conditions and physical spawning habitat of Chinook salmon in riffle-pool units and found that 1D models over-predict fish habitat quality. By comparing depth, velocity, and shear velocity predictions from a 2D model at the 1-m scale to field measurements, Pasternack et al. [41] found the numerical model to result in depth and velocity prediction errors of 21% and 29%, respectively. A recent study compares the performance of 2D and 3D hydrodynamic models for instream habitat modelling, concluding that the use of a three-dimensional model leads to significantly improved results Pisaturo et al. [44]. However, it is questionable if 3D models will find soon wide application in hydropeaking impact assessment at reach scale, due to high computational costs.

To the authors' best knowledge, no studies provide a systematic overview over the suitability of 1D and 2D hydrodynamic models for hydropeaking impact assessment with different ERHPs and for habitat quality and quantity, for a range of river morphologies and spatial resolutions of the computational domains. Therefore, we address this knowledge gap by comparing the 1D and 2D hydrodynamic model of the numerical software BASEMENT v2.7 [53] as input for the computation of some ERHPs, namely the dewatering velocity, the wetted area at peak and base flow and the bed shear stress, and also of habitat suitability for three different life stages of brown trout (spawning areas, juvenile and adult). Furthermore, the influence of the spatial resolution of the 1D and 2D models on the given metrics is quantified. The comparison is done under the consideration of three different river planforms, an alternating bar, a wandering and a braiding morphology, representative of Alpine rivers. Recommendations regarding the required model dimensionality and spatial resolutions are established for different ERHPs and with respect to the morphological complexity of the river reach under consideration.

2. Methods

For the conducted analysis we define a characteristic hydropeaking event and generate the computational domains based on three different river planforms. These serve as input for the 1D and 2D simulations performed with the numerical software BASEMENT v2.7 [53]. Based on the simulated hydraulic variables, namely the water depth and the flow velocity, different ERHPs are computed. The ERHP results obtained from the 1D and 2D models are compared for different spatial resolutions, where the finest resolved 2D model is considered the most accurate solution and is therefore regarded as the reference scenario (benchmark). When comparing 1D and 2D hydrodynamic models as input for a hydropeaking impact analysis we hypothesize that the hydrodynamic modelling results (flow velocities and flow depths) exhibit increasing accuracy by increasing the (i) model dimensionality (1D/2D) [41] and (ii) spatial resolution of the computational domain [27, 17, 39]. The numerical model results are thus not compared to experimental or field data. A similar approach was followed by Vanzo et al. [52]. Investigations using a 3D model are typically limited to small river sections due to high computational costs and are not considered in this study. The workflow is illustrated in Fig. 1.

2.1. Channel Morphologies

River morphological complexity is expected to affect both ecological impacts from hydropeaking [e.g. 52] and numerical model performance [e.g. 24, 4]. Therefore, we consider three river planforms with morphological characteristics representative for regulated Alpine rivers, namely an alternating bar, wandering [13] and braiding morphology. Similar river morphologies can be found along the approximately 90 kilometer long section of the Alpine Rhine between Tamins, Switzerland and the estuary of Lake of Constance. Similar to previous studies [e.g. 52, 50], we utilize digital elevation models (DEM) of three laboratory flumes from Garcia Lugo et al. [15] with a channel of 14.5 m length and 0.3 m, 0.8 m and 1.5 m width, respectively. To obtain spatial scales typical for Alpine rivers, the DEM were upscaled by a factor of $\lambda = 100$ as in Vanzo et al. [52] and the mean bed slope was corrected to 3‰. The detrended channel planforms are depicted in Fig. 2.

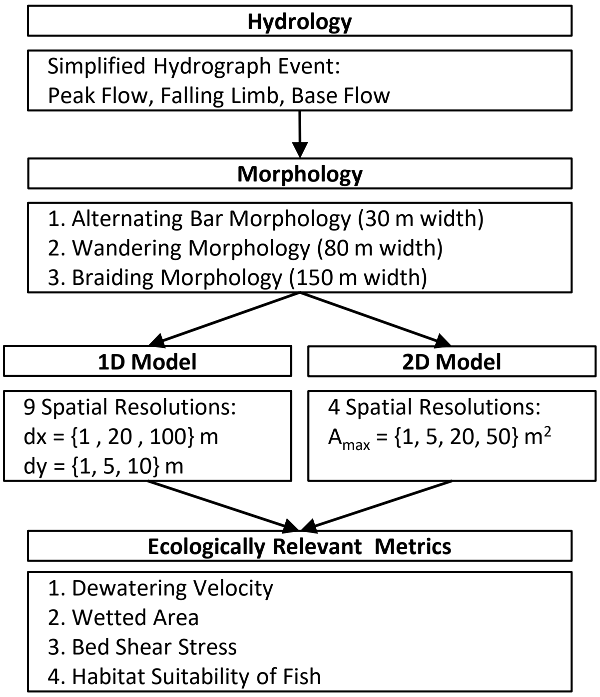

Figure 1: Overview of adapted workflow including the definition of a characteristic hydropeaking event, the three morphological planforms, the 1D and 2D hydrodynamic numerical models with varying spatial resolutions and the considered ecologically relevant hydraulic parameters.

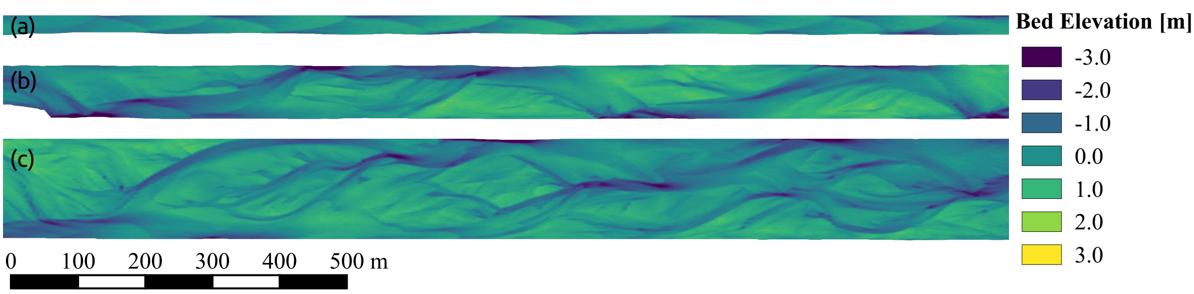

Figure 2: Bed elevation of the finest resolved 2D computational grids detrended with the longitudinal slope of the (a) alternating bar, (b) wandering and (c) braiding morphology.

2.2. Numerical Model Setup

The hydrodynamic simulations were performed with the software BASEMENT (v2.7) [53]. BASEMENT solves the unsteady 1D de Saint-Venant equations and the 2D shallow-water equations. For details on the mathematical and numerical models we refer to the software manual [54].

For the 2D scenarios, the hydraulic roughness was set to 31 $m^{1/3}s^{-1}$ (Strickler parametrization). To minimize the deviations between 1D- and 2D-results originating from different numerical treatment of bed roughness, the Strickler coefficients of the 1D models were determined in a calibration process by minimizing the difference in the water surface elevation (WSE) between the finest resolved 1D and 2D model for bankfull discharge conditions. Thereby, Strickler values of 27.7, 28.5 and 29.0 $m^{1/3}s^{-1}$ were determined for the alternating bar, wandering and braiding morphology, respectively.

Simulation time was set to 10.33 hours, matching the hydrograph duration (cf. Supplementary Material 1), and simulations were run in parallel computing, using a 16-cores Intel Xeon E5-2667 v3 (3.20GHz) processor unit.

2.2.1. 2D Computational Domains

For each morphology, four unstructured triangular grids with varying spatial resolution were generated with the QGIS plugin BASEmesh [54]. The series of four grids have mean (maximum) element size A_{mean} (A_{max}) of 0.63 (1), 6.0 (10), 12 (20), and 27 (50) m^2, respectively. Finer mesh resolutions were not considered here, as the benefit of a mesh refinement to a spatial resolution finer than the input topographic data is debatable. We therefore considered the finest resolution (mean size of 0.62 m^2) as a reference in this study. However, it is worth mentioning that also 2D model results with high spatial resolutions (1 m scale) can still exhibit non-negligible deviations in comparison to field measurements. For riffle-pool sequences with complex 3D features, Pasternack et al. [41] reported mean prediction errors for depth and velocity of 20% and 30%, whilst Papanicolaou et al. [40] found errors below 10% and 25%, respectively. The coarsest spatial resolution (mean size of 27 m^2) was indicatively chosen as upper limit for a sufficient representation of the morphological features.

2.2.2. 1D Computational Domains

The computational domains for the 1D simulations are based on cross sections. To minimize topographical deviations in comparison to the finest resolved 2D grids ($A_{max} = 1\ m^2$), the finest resolved 2D grids were converted into regularly spaced digital elevation models with point spacing of 1 m, respectively. Subsequently, cross section based computational domains were extracted with three different spatial resolutions in longitudinal (1, 20, 100 m) and transversal direction (1, 5, 10 m), respectively, resulting in nine 1D domains for each morphology.

2.2.3. Error in Topographic Representation

For each of the 1D and 2D computational domains, the error in topographic representation compared to the finest resolved 2D computational grid (reference) was quantified by the area weighted mean absolute error (MAE). Therefore, bed elevations of each computational domain were resampled at the element center locations of the reference grid and the MAE was computed as,

$$MAE_z = \frac{\sum_{i=1}^{N} A_{i,ref} \cdot (|z_i - z_{i,ref}|)}{\sum_{i=1}^{N} A_{i,ref}} \tag{1}$$

where z_i are the bed elevations resampled at the center locations of element i of the reference grid, $z_{i,ref}$ and $A_{i,ref}$ are the bed elevations and element areas of the reference grid and N is the number of elements in the reference grid.

2.2.4. Characteristic Hydropeaking Event

A hydropeaking event was designed by simplifying and downscaling an observed hydrograph from the gauging station Domat/Ems, Switzerland on the Alpine Rhine, while preserving observed key characteristics such as the ratio between peak and base flow of five and the recession rate of 0.75 $m^3s^{-1}min^{-1}$. The downscaling of base and peak flow magnitudes was performed such that the alternating bar morphology exhibits emerging sediment banks during base flow, while being completely inundated during peak flow conditions, since such flow conditions are observed on the Alpine Rhine. During the defined base flow of 15 m^3s^{-1} a significant part of the river bed remains dry in all three morphologies, representing typical environmental flow conditions downstream of storage HPP. During peak flow conditions of 75 m^3s^{-1}, the alternating bar morphology is bankfull, while some river bed area remains dry in the wandering and braiding morphologies. The duration of constant base or peak flow was chosen sufficiently long for the hydrodynamic simulations to reach quasi steady-state conditions. Further information on the hydrograph are presented in the Supplementary Material 1. The hydrograph serves as input on the upstream boundary conditions for all three morphologies. The occurrence of different channel morphologies along one river reach (i.e. with the same hydrograph) is a valid assumption, as for example on the Alpine Rhine river morphology changes from a braiding or wandering morphology in the riparian river reach in Mastrils, Switzerland to an alternating bar morphology within several kilometers. The assumption is reasonable also in case of river restoration projects targeting at modifying reach scale morphologies, but with same hydrological regime.

2.3. Ecologically Relevant Hydraulic Parameters (ERHPs)

In this study, we focus on a set of ERHPs that are hydropeaking sensitive, namely: (a) the vertical dewatering velocity, (b) the wetted area at peak and base flow and (c) the bed shear stress.

2.3.1. Vertical Dewatering Velocity

The vertical dewatering velocity during the falling hydrograph limb was calculated as the decrease in water depth Δh in a defined time interval Δt [23] given by Eq. 2.

$$V_{dewatering} = \Delta h / \Delta t \tag{2}$$

In this study, the vertical dewatering velocity was calculated for time intervals of five minutes between the start of the falling limb of the hydrograph and the time when again steady-state base flow conditions are reached. For the 1D simulations, the vertical dewatering velocity was calculated for each cross section [2]. Similarly, for the 2D model results the dewatering velocity was calculated for defined transversal slices of 1 m. For each cross section (1D) or slice (2D), the maximum dewatering velocity during the considered time period was determined, since on a local scale increasing vertical dewatering velocities have been associated with a higher stranding risk [20]. For the comparison of dewatering velocities between different simulations (reach scale), the median dewatering velocity was determined based on the maximum values of all cross sections or slices, respectively [2, 47].

2.3.2. Wetted Area at Peak and Base Flow

For the 1D simulations, the wetted area A_{wet} was computed by multiplying the wetted perimeter of each cross section with its longitudinal extent, which corresponds to the longitudinal cross section spacing, and half of the longitudinal cross section spacing for the first and last cross sections, respectively. For the 2D simulations, the wetted area was obtained by summing up the area of all wetted elements. The wetted area was evaluated based on flow depths larger than a minimum flow depth of 1 cm, corresponding to the minimum flow depth selected in the numerical model to avoid numerical instabilities.

2.3.3. Macroinvertebrate Drift

The rapid increase in discharge during hydropeaking events is known to cause disturbances of the river bed and is associated with catastrophic drift of bottom-dwelling benthic species [18, 10, 11]. Catastrophic drift is closely linked to the increase in near-bed shear stress as a result of increased flow velocities [18]. Following previous studies [25, 52], we consider near-bed shear stress τ_B as a proxy indicator for macroinvertebrate drift. The bed shear stress was evaluated in each cell of the 2D grids and on each point along the cross sections of the 1D computational domains with the Strickler parametrization for wide channels ($B/h > 10$):

$$\tau_B = \rho g \frac{U^2}{k_{St}^2 h^{1/3}} \tag{3}$$

where ρ is the density of water, g is the gravitational acceleration, U is the local flow velocity magnitude, k_{st} is the Strickler roughness coefficient, h is the local flow depth and B is the channel width. This simplified expression for the bed shear stress for wide channels holds in this study as $B/h > 10$ was fulfilled in all morphologies. The mean absolute errors (MAE) of the predicted bed shear stress τ_B w.r.t. to the finest resolved 2D model were calculated as described by Eq. 1. Further, the relative MAE was obtained by normalizing the MAE of a scenario with the mean bed shear stress of all elements obtained with the finest resolved 2D simulation.

2.4. Habitat Suitability of Fish

Together with previous ERHPs, we evaluate also fish habitat suitability, following a well-established procedure. Habitat quantification is assessed in terms of weighted usable area (WUA) for juvenile and adult brown trout as well as for spawning areas of brown trout (common target species in Alpine rivers). For the three life stages in consideration, univariate preference functions for flow depth and flow velocity were applied (see Fig. 4). The preference functions from Hauer et al. [26] were used for juveniles, while for adults and spawning areas, the preference functions from Person [43] were applied. The weighted usable area $WUA_{Q,s}$ for given flow Q and life stage s, reads

$$WUA_{Q,s} = \sum_{i=1}^{N} A_{i,Q} CSI_{i,Q,s}, \tag{4}$$

where $A_{i,Q}$ is the surface area of computational element i and $CSI_{i,Q,s}$ is the composite suitability index of the i^{th}element. The latter is calculated as the product of the univariate suitability index for the flow depth $SI_{i,Q,s,h}$ and the flow velocity $SI_{i,Q,s,v}$ ([6]):

$$CSI_{i,Q,s} = SI_{i,Q,s,h} \cdot SI_{i,Q,s,v}. \tag{5}$$

It is important to recall that habitat quantity and quality depend also on the chosen biological model, and not only on the underlying ERHPs (e.g. flow and depth distributions). Differences arising from the choice of alternative biological models are beyond the scope of this work.

3. Results

3.1. Topographic Representation

In Fig. 3, the error in the topographic representation is illustrated as a function of the longitudinal cross section spacing dx for the 1D scenarios and as a function of the equivalent length L_{eq} for the the 2D scenarios. The equivalent length L_{eq} for each 2D scenario is determined as $L_{eq} = \sqrt{\frac{4}{3} A_{max}}$ and corresponds to the edge length of an equilateral triangle with an area equivalent to that of the maximum element size of the respective 2D grid. For the finest resolved 2D models, L_{eq} takes a value of 1.155 m. As expected, the error in the topographic representation of the 1D computational domains increases with increasing longitudinal cross section spacing dx, but also with increasing transversal point spacing dy (Fig. 3). For the 2D grids,

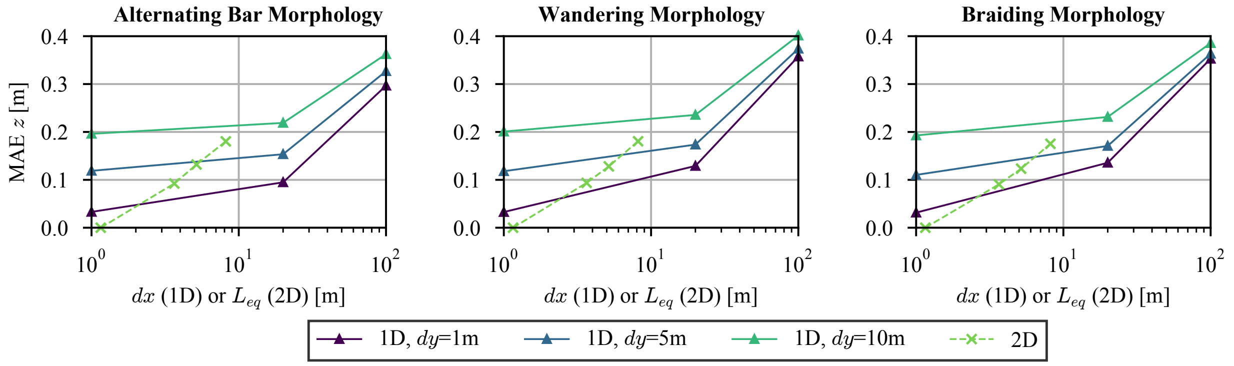

Figure 3: Mean absolute errors (MAE) in the bed elevation of the 1D and 2D computational domains in comparison to the finest resolved 2D grids.

the topographic error increases with larger maximum element size. The topographic errors of the 2D grids are comparable to those of the finer resolved 1D computational domains, whereas the topographic error of the 1D domains with the largest longitudinal spacing of $dx = 100$ m is approximately twice the error of the coarsest 2D grid.

3.2. Hydraulic Variables

In Fig. 4, the depth and velocity distributions resulting at steady-state base and peak flow conditions in the 30 m wide alternating bar morphology, the 80 m wide wandering and the 150 m wide braiding morphology are presented for 1D and 2D simulations with the finest and coarsest spatial resolution, respectively. For the sake of conciseness, the results of the simulations with intermediate spatial resolutions are omitted. For a given flow condition and morphology, the 1D models reproduce a significantly smaller range of flow velocities and larger median flow velocities than the 2D models. The deviations from the finest resolved 2D models increase with larger cross section spacing d_x, while the lateral point spacing d_y has a less significant impact. For the 2D scenarios, the range of represented flow velocities and the median flow velocities slightly decrease for the coarser spatial resolution. Flow depth distributions are less sensitive to model dimensionality and spatial resolution than flow velocity distributions. Median flow depths slightly increase with coarsening spatial resolution for the 2D model and slightly decrease for the 1D model, respectively.

The mean absolute errors (MAE) of the predicted flow velocities magnitudes U and flow depths h w.r.t. to the finest resolved 2D model were calculated in the same manner as the MAE of the bed elevation described by Eq. 1 and are illustrated in Fig. 5 as a function of the longitudinal cross section spacing dx and the lateral profile resolution dy for the 1D scenarios and as a function of the equivalent length L_{eq} for each 2D scenario. The 1D simulations result in significantly larger flow velocity errors than any of the 2D simulations. An exception to this poses the alternating bar morphology at peak flow conditions, where all considered scenarios result in a similar flow velocity error. Further, the velocity errors of the 1D models

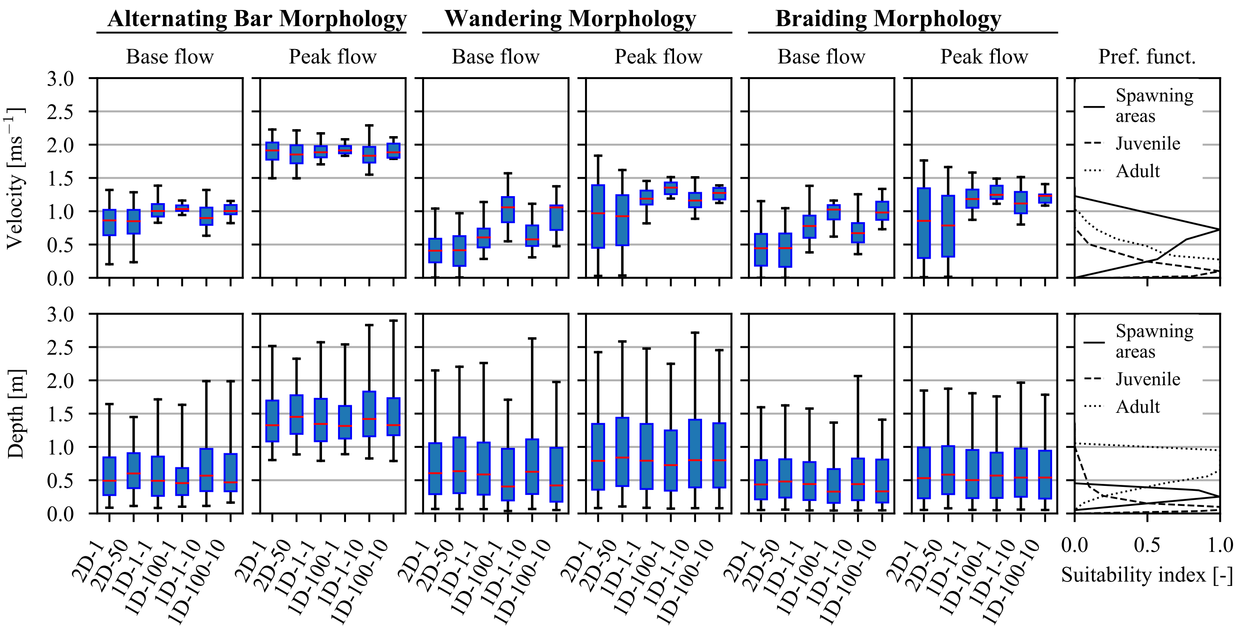

Figure 4: Simulated velocity and depth distributions at base and peak flow conditions in all three considered morphologies for the finest and coarsest resolved 1D and 2D scenarios. The boxes are limited by the lower and upper quartile values and include the median (red). The whiskers indicate the five and 95 percentiles. For 2D scenarios the maximum element area is indicated by «2D-A_{max}» and for 1D scenarios the longitudinal (dx) and lateral (dy) spacing is given as «1D-dx-dy». The habitat suitability index (SI) curves for spawning areas, juvenile and adult brown trouts are illustrated for reference.

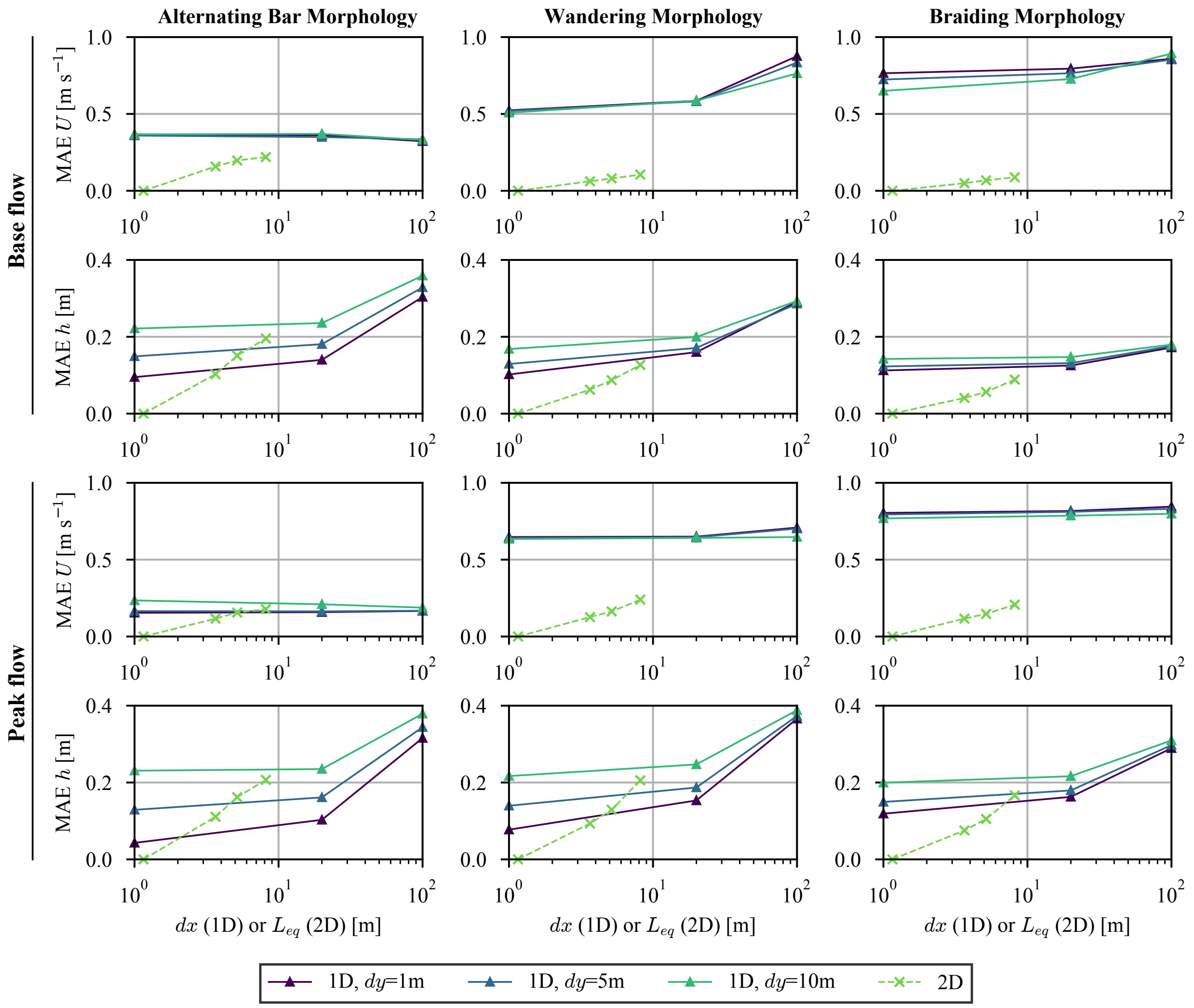

Figure 5: Mean absolute errors (MAE) in simulated velocities magnitudes U and flow depths h obtained with the 1D and 2D scenarios in comparison to the finest resolved 2D scenarios.

are significantly larger in the wandering and braiding morphology, than in the alternating bar morphology. In contrast, flow velocity errors of the 2D models are similar across all three morphologies. While the 2D models exhibit a clear trend of larger flow velocity errors with coarser spatial resolution, this is not true for the 1D models. As expected, the depth error increases with coarser longitudinal and lateral resolution (1D) and increasing equivalent element length (2D). However, 1D models with a longitudinal resolution of 1 m and 20 m perform similarly well or better than the coarser resolved 2D simulations, with exception for base flow conditions in the braiding morphology.

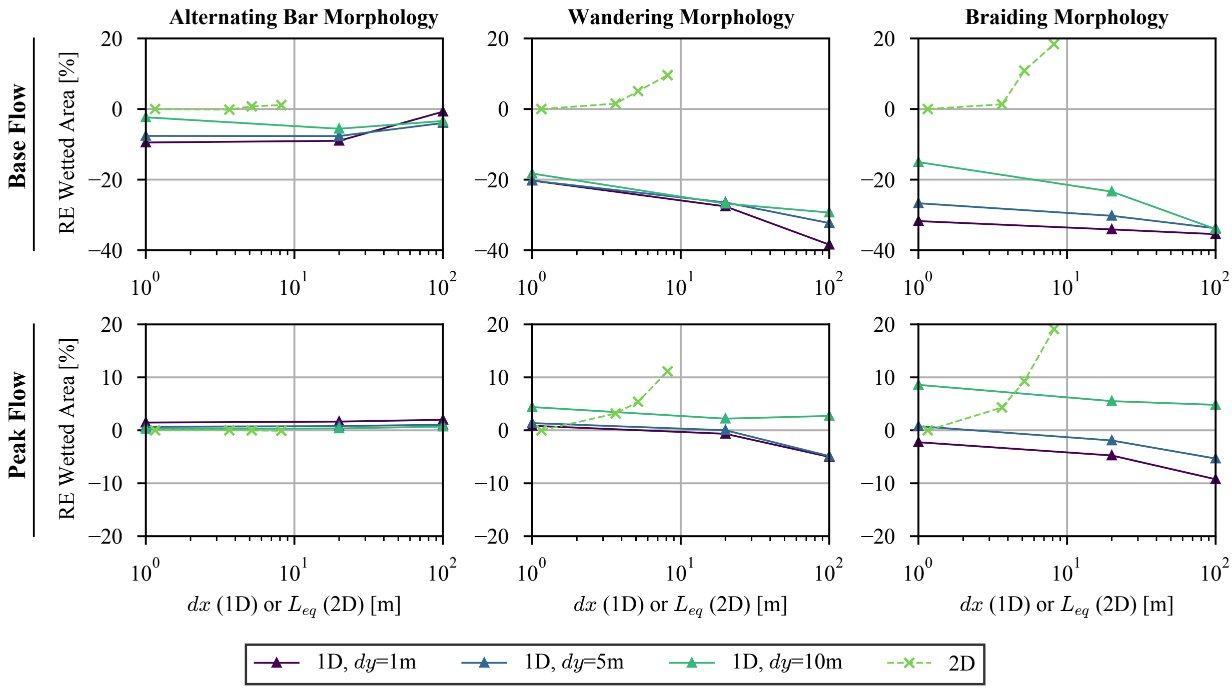

Figure 6: Relative errors (RE) in the wetted area at base and peak flow conditions in comparison with the finest resolved 2D simulation as a function of the longitudinal dx and lateral spacing dy for the 1D scenarios and of the equivalent length L_{eq} for each 2D scenarios.

3.3. Wetted Area

The relative errors (RE) in the predicted wetted area at base and peak flow conditions are represented for all three morphologies in Fig. 6. In the alternating bar morphology, the relative errors of both 1D and 2D models are comparable, especially at the almost completely inundating peak flow conditions. Moreover, the relative errors remain comparable for varying spatial resolutions. In the more complex morphologies, the relative error is significantly affected by model dimensionality and spatial resolution. While the coarser resolved 2D models generally result in an overestimated wetted area, 1D models tend to result in an underestimation. Further, the deviation between 1D and 2D models is more distinct during base flow conditions, where the 1D scenarios result in significantly larger errors. At peak flow conditions the 1D and 2D models result in a similar range of errors below ±20%. For the 2D models, the relative error increases with increasing element size. For the 1D scenarios, the relative error mostly increases with increasing longitudinal cross-section spacing, while a finer spatial resolution in lateral direction does not necessarily reduce the relative error.

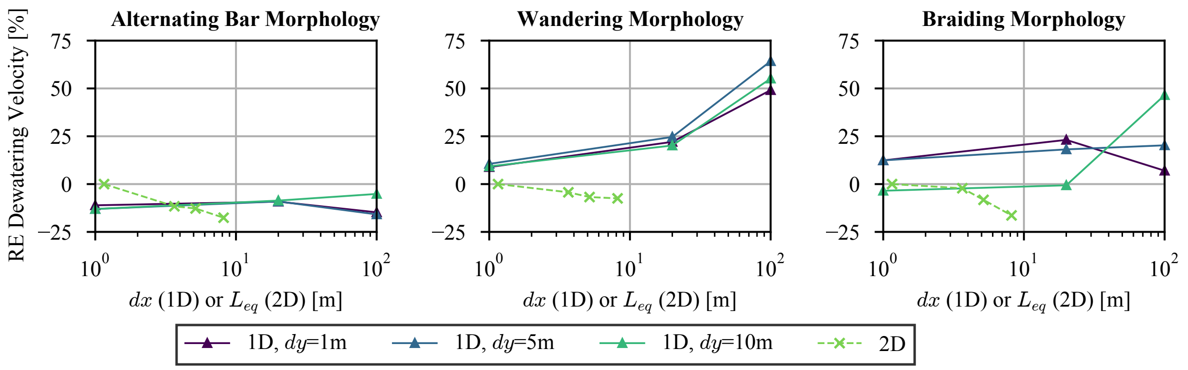

Figure 7: Relative errors (RE) in the dewatering velocity in comparison with the finest resolved 2D simulation as a function of the longitudinal dx and lateral spacing dy for the 1D scenarios and of the equivalent length L_{eq} for the 2D scenarios.

265 *3.4. Dewatering Velocity*

266 The RE in the dewatering velocity with regard to the finest resolved 2D simulation are compared for all scenarios in Fig. 7. In the alternating bar morphology, all scenarios underestimate the dewatering velocity in comparison to the finest resolved 2D simulation, but RE remain below 25%. In the wandering morphology, the 1D models with 1 m longitudinal cross section result in a similar RE as the coarser resolved 2D models. However,the relative error increases significantly with increasing longitudinal cross section spacing, reaching 25% for cross section spacings dx of 20 m and 50% for dx of 100 m, respectively. For the most complex braiding morphology, the 1D and 2D models result in a similar range of errors, mostly with below ±25% with exception of the 1D scenario with the coarsest spatial resolution.

274 *3.5. Bed Shear Stress*

275 Generally, the 1D scenarios result in large relative mean absolute errors (MAE), above 80% and even up to 280% (Fig. 8), with exception of peak flow conditions in the alternating bar morphology, where the relative MAE is approximately 20%. Also the coarser resolved 2D scenarios result in significant errors between 30% and 80%. In most cases, the relative MAE increase with coarser spatial resolution, for both 1D and 2D models. Further, the relative MAE are generally larger at base flow than at peak flow conditions.

280 *3.6. Habitat Suitability of Fish: Weighted Usable Area (WUA)*

281 The relative errors (RE) of the predicted WUA for adult brown trout in comparison to the finest resolved 2D scenarios are illustrate in Fig. 9. The WUA during peak flow conditions in the alternating bar morphology was zero for all models, since the simulated flow velocities lie outside the range of the preference functions (Fig. 4). Hence, this comparison is omitted in Fig. 9.

285 The RE of the finest resolved 1D models range between −55% and −71% at base flow and between −95% and −100% at peak flow conditions. In the alternating bar morphology, the 1D models with a lateral

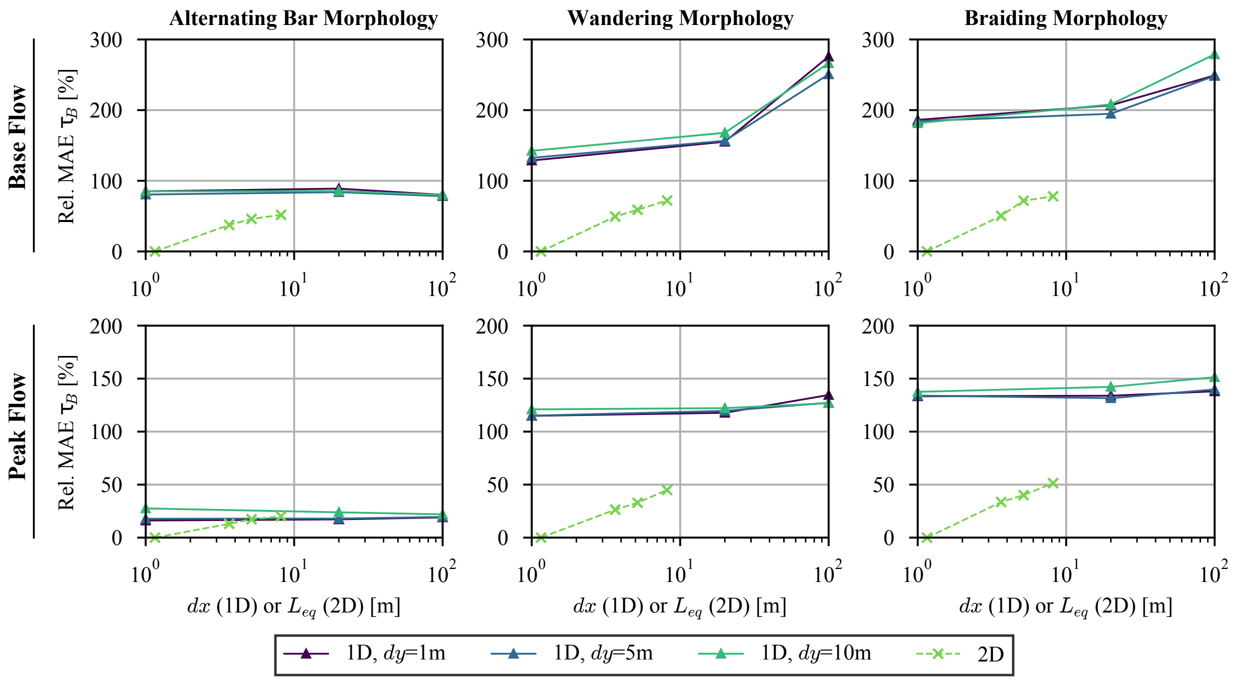

Figure 8: Relative mean absolute error (MAE) in the bed shear stress in comparison with the finest resolved 2D simulation as a function of the longitudinal dx and lateral spacing dy for the 1D scenarios and of the equivalent length L_{eq} for each 2D scenarios.

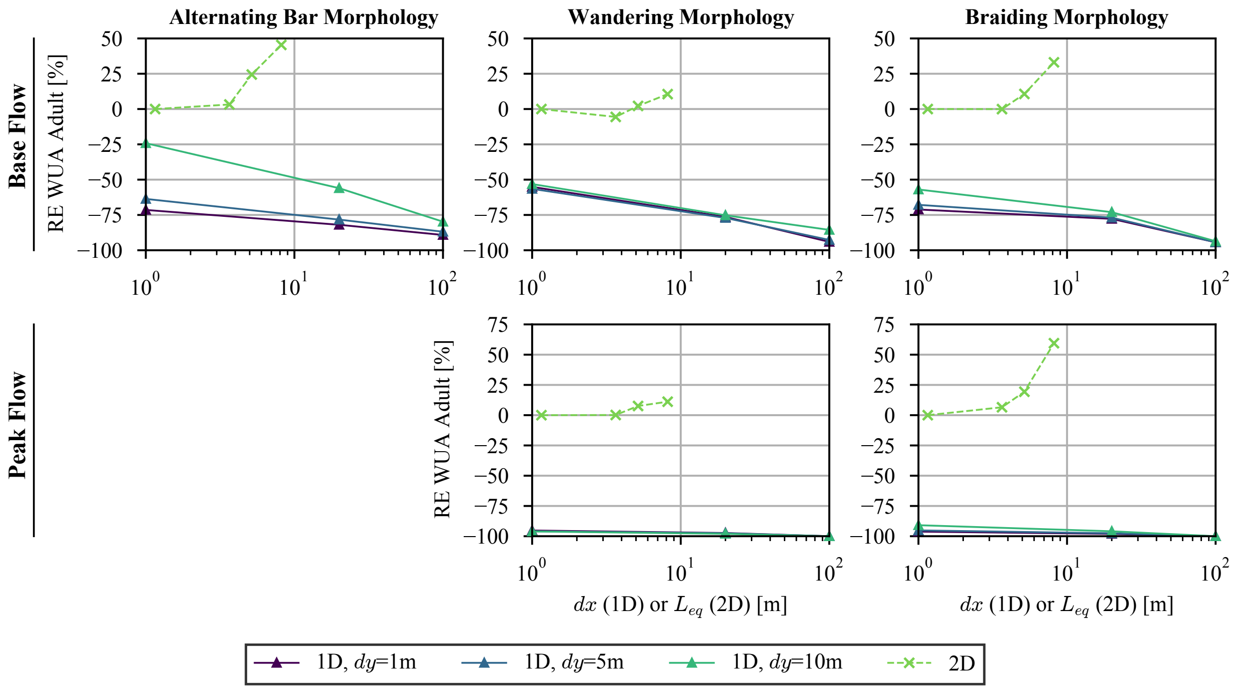

Figure 9: Relative errors (RE) in the weighted usable area of adult brown trout in comparison with the finest resolved 2D simulation as a function of the longitudinal dx and lateral spacing dy for the 1D scenarios and of the equivalent length L_{eq} for each 2D scenarios.

resolution dy of 10 m result in smaller errors than the simulations with dy of 1 m and 5 m. The WUA calculated from 2D model results with A_{max} of 10 m^2 (L_{eq} of 10.8 m) exhibits RE between −6% and 3%. However, a further coarsening of the spatial resolution of the 2D model significantly affects WUA prediction, resulting in RE up to 59%.

Due to the similarity with the results for adult brown trout, the results for the WUA for spawning areas of brown trout and juvenile brown trout are omitted here for the sake of conciseness and are instead included in the Supplementary Material.

3.7. Computational Effort

The computational runtime of the simulations with a duration of 10.33 hours varies over seven orders of magnitude, where the coarsest resolved 1D simulation in the alternating bar morphology requires only 0.07 s, while the finest resolved 2D simulation in the braiding morphology requires almost 16 hours. The applied numerical models [53] make use of explicit time integration schemes, for which the computational runtime scales exponentially with the number of computational elements due to stability constraints [e.g. 48]. Despite the simplified mathematical equations of the 1D model in comparison to the 2D model, the finest resolved 1D model (dx = 1m, dy = 1m) requires runtimes in the same order of magnitude ($\sim 10^3$ s) as the second finest resolved 2D model ($A_{max} = 10$ m^2) within the same morphology. Unsurprisingly, the runtime of both 1D and 2D models can be further reduced with a coarser spatial resolution. The computational speedup in comparison to the finest resolved 2D simulations obtained by reducing the spatial resolution of the 2D models range between 30 and 430, while for the 1D models speedups between 22 and 563'787 are achieved.

4. Discussion

The relative deviations of the considered metrics in comparison to the finest resolved 2D models and the performance in terms of computational effort are summarized in Fig. 10. The 1D and 2D scenarios with varying spatial resolutions are distinguished by columns, while the three morphologies are distinguished into horizontal sections. The relative deviations are classified into 7 categories, for which the deviation from the finest resolved 2D scenarios ($A_{max} = 1\ m^2$) is indicated by colors ranging from green (small deviation) to red (large deviation). Further, under- and overestimations are indicated by minus (-) and plus (+) signs, respectively. The results are discussed below.

4.1. Hydraulic Variables: Flow Depth and Velocity

For a given morphology and flow condition, the mean absolute errors (MAE) of flow velocities simulated with the 1D models are larger than those simulated with any of the considered 2D models. Further, the MAE of the velocities simulated with the 1D models generally increase with incrementally complex morphology and with reduced discharge (Fig. 5). The fact that median flow velocities of 1D models generally decrease with incrementally complex morphology and with reduced discharge (Fig. 4), highlights that the velocity predictions with 1D models are strongly affected by the morphological complexity and the discharge conditions. In contrast, the MAE of the flow depths simulated with 1D models do not vary noticeably with the river morphology and the flow conditions. For the 2D models, the MAE of both velocity and flow depth decrease with increasingly complex morphology. This in combination with the trend to smaller flow depths and velocities in the more complex morphologies indicates that the river morphology has a significantly smaller impact on the prediction accuracy of the flows depths and velocities for 2D models than for 1D models.

The observed trends are not surprising, since in more complex morphologies, as well as during low discharge flow conditions, morphological structures such as sediment bars emerge through the water surface and may significantly affect the local flow and tend to induce 2D or even 3D flow patterns. The ability to resolve such flow structures with the numerical model decreases with reduced model dimensionality and with coarser spatial resolution. Increased model sensitivity to topographic input data for low discharge flow conditions and in the presence of morphological features which induce a topographic steering effect was also

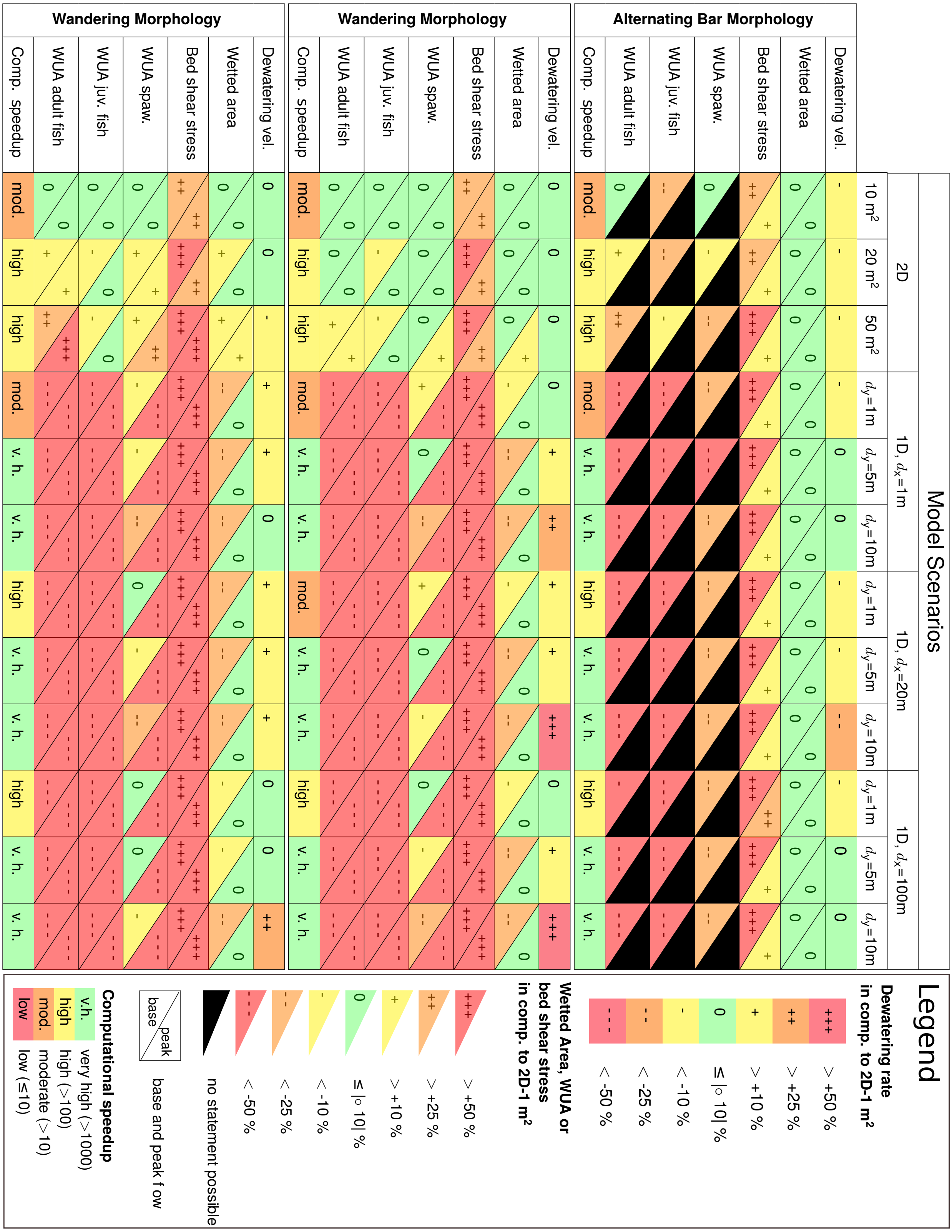

Figure 10: Summarized overview of the relative deviations and computational speedups obtained with the different modelling scenarios in comparison to the finest resolved 2D model.

observed in previous studies [8, 33]. Moreover, in 1D models flow is not routed between two subsequent cross sections, but instead a constant WSE based on conveyance is computed for each cross section. Therefore, the naturally occurring flow paths captured in the 2D model may not be fully depicted by the 1D models.

Considering the above limitations, the observation that 1D simulations exhibit significant deviations in terms of simulated flow velocity compared to the finest resolved 2D simulations is not surprising and corresponds with with findings of Benjankar et al. [4] and Gibson and Pasternack [19]. The aforementioned findings are not true for the alternating bar morphology at peak flow conditions, where all considered scenarios result in a similar flow velocity error. We assume the small differences are the result of the completely inundated peak flow conditions, which result in a predominantly 1D flow pattern.

For both 1D and 2D models, the MAE of flow depths and velocities generally increase with coarser spatial resolutions. However, for the velocity obtained with 1D models the MAE are much less affected by the lateral resolution dy than by the longitudinal resolution dx, presumably due to the cross sectionally-averaged nature of the 1D model. Nevertheless, it is doubtful whether the hydraulic conditions can be predicted with sufficient robustness when e.g. the 30 m wide alternating bar morphology is resolved by approximately 4 stencils in lateral direction for the coarsest lateral resolution $dy = 10$m.

Further, we found that the range of simulated flow velocities is substantially smaller for 1D than for 2D models, as a consequence of the cross sectionally-averaged nature in the 1D model (Fig. 4). This is in agreement with findings of Brown and Pasternack [8]. Similarly, coarser spatial resolution effectuates a spatial averaging effect and reduces a model's ability to resolve local velocity variations, resulting in smaller ranges of simulated flow velocities (Fig. 4).

4.2. Wetted Area and Dewatering Velocity: A Proxy for Fish Stranding

In the alternating bar morphology, the relative error for the wetted area is below $\pm 10\%$ for both 1D and 2D models and is not significantly influenced by the spatial resolution (Fig 6). This is not surprising, since during peak flow conditions, the water level is approximately at the height of the sediment bars and the entire channel is inundated. Further, the alternating bar morphology is characterized by one main flow path, which may explain the insensitivity to the model dimensionality and the spatial resolution also during base flow conditions. In the more complex wandering and braiding morphologies, the relative errors of the 1D and 2D models diverge. While the 1D models underestimate the wetted area in comparison to the finest resolved 2D models, the coarser 2D models result in an overestimation. The underestimation of the wetted area with 1D models is in agreement with their tendency to underestimate the flow depths (Fig 4). Similarly, the coarser resolved 2D models tend to overestimate the flow depths in comparison to the finest resolved 2D models and consequently also overestimate the wetted area.

For peak flow conditions, the finest resolved 1D model results in small relative errors of the wetted area in all three morphologies (RE $< 5\%$). However, the significant underestimations of -20% in the wandering and −32% in the braiding morphology for base flow conditions indicate that a 1D model is not well suited for the prediction of the wetted area in complex river morphologies with emerging topographical features or multiple flow paths.

In the wandering and braiding morphology, the only minor deviations (RE $< 5\%$) in the wetted area were observed when increasing the maximum element area of the 2D model from 1 m^2 to 10 m^2. A further increase of the maximum element area to 20 m^2 or 50 m^2 is not recommended, since deviations in the wetted area in comparison to the finest resolved 2D model exceed 10% (Fig. 10).

Accurate predictions of the vertical dewatering velocity mainly depend on the simulation of the spatial and temporal WSE distribution. As shown in Fig. 3, the finest resolved 1D models exhibit a small error in the topographic representation ($<$ 5 cm) and are reasonably well capable of reproducing flow depths distributions obtained with the finest resolved 2D models, with MAE around 0.1 m, both at base and peak flow conditions. Therefore, also the error in the spatial WSE distribution is expected to be moderately small. This is to some extent reflected in the acceptably small relative errors (RE $< 25\%$) in the dewatering velocity obtained with the finest resolved 1D model across all three morphologies (Fig. 7). In the more complex morphologies, increasing the spatial resolution of the 1D models results in significantly deviating dewatering velocities and less robust results. Hence, a high-resolution 1D model may suffice for the prediction of the dewatering velocity within a relative error of $\pm 25\%$, even in more complex morphologies. The fact, that a coarser lateral resolution dy of 10 m results in a smaller relative error than the finer lateral resolution, should not be interpreted as improved prediction accuracy, but indicates a divergence of the model results due to an oversimplification of the topography. The vertical dewatering velocity calculated from the 2D model results is sensitive to the mesh resolution. However, all considered mesh resolutions predict the vertical dewatering velocity with less than 25% deviation from that of the finest resolved 2D model (Fig. 10). The effect of the river morphology on the relative error of the dewatering velocity appears to be negligible for the 2D model.

Methods for quantifying fish stranding risk typically rely on predictions of both the wetted area and vertical dewatering velocities [e.g. 32, 31]. Therefore, a 1D model might not be adequate for the quantification of fish stranding risk in more complex river morphologies and during low flow conditions, mainly due to the limited accuracy of predicting the wetted area. A 2D model appears to be the more adequate choice for the prediction of the wetted area and for fish stranding risk assessment.

4.3. Macroinvertebrate Drift: Bed Shear Stress

Bed shear stress is proportional to the squared flow velocity and to the inverse flow depth (2.3.3). Consequently, error propagation for the bed shear stress predictions is non-linear and over-proportionally affected by errors in the simulated flow velocities. Since the 1D models tend to overestimate flow velocities and underestimate flow depths in comparison to the finest resolved 2D model, observed bed shear stress errors are particularly large. As indicated in Fig. 10, none of the 1D scenarios or coarser resolved 2D scenarios result in a relative error under ±25%, except during fully inundating peak flow conditions in the alternating bar morphology. Therefore, we recommend the use of a highly resolved 2D model with a maximum element area in the order of ∼1 m^2 or finer, for hydropeaking related analysis for which the bed shear stress as a proxy for macroinvertebrate drift is of interest.

4.4. Habitat Suitability of Fish: Weighted Usable Area

For juvenile and adult brown trout, the weighted usable areas (WUA) obtained from the 1D scenarios are significantly underestimated in comparison to the WUA computed from the model results of the finest resolved 2D scenarios, with relative errors between −50% and −100% (Fig 10). The large deviations can be attributed to a combination of three factors, as 1D models (i) generally exhibit a smaller range of occurring flow velocities due to the cross sectionally-averaged nature of the 1D model and (ii) tend to overestimate the flow velocities in comparison to the finest resolved 2D model (Fig. 10). Additionally, (iii) the univariate preference functions for juvenile and adult brown trout require relatively small flow velocities below 1 ms^{-1}. In contrast, the WUA for spawning areas of brown trout can be more accurately predicted from the model results of the finest resolved 1D model (RE > -25%), since the preference function for the spawning areas requires larger flow velocities that tend to coincide with the range of flow velocities predicted by the 1D models. This indicates that 1D models are not robust tools for predicting habitat suitability of fish based on univariate preference functions for the flow velocity due to their limited ability of distinguishing lateral velocity variations. This even more so holds for cases where the spatial distribution of habitat is of interest. The significant deviations between habitat predictions based on 1D and 2D model results are in agreement with findings of Brown and Pasternack [8], that global habitat suitability indices (GHSI) in riffle-pool units differ substantially when calculated from 1D and 2D models. In contrast to the significant discrepancies found in our study, Benjankar et al. [4] only observed small differences in WUA obtained from 1D and 2D modelling reach scale. However, Benjankar et al. [4] used 1D models results as input to the fish habitat model CASiMIR [38] to generate spatially distributed, local velocities and thereby circumvent the major limitation of the 1D model.

Increasing the maximum element area of the 2D model from 1 m^2 to 10 m^2 has in most cases only an insignificant effect on the predicted WUA of spawning areas of brown trout and juvenile and adult brown trout, regardless of the morphology (Fig. 10), but can reduce computational costs by one order of magnitude. A further reduction of the spatial resolution tends to result in significant under- and overestimations of the WUA in comparison to the finest resolved 2D scenarios, since a reduced spatial resolution limits the model's ability to reproduce complex flow structures, such as horizontal eddies and recirculating zones. Based on the results in Fig. 10, a 2D model with a spatial resolution with maximum element areas between 1^2 or 10 m^2 is recommended for hydropeaking related evaluations based on habitat suitability in terms of weighted usable area.

5. Conclusions

In this study, we evaluate the performance of different 1D and 2D hydrodynamic model setup by comparing derived hydropeaking-sensitive ecologically relevant metrics. In particular, the influence of the spatial resolution of the 1D and 2D models on the final results was quantified and evaluated. The analysis was conducted on three different morphologies: alternating bar, wandering and braiding morphology.

Our results indicate that 1D models with a high spatial resolution of about ~1 m, allow the prediction of the vertical dewatering velocity and wetted area with a relative error compared to a 2D model below ±25% when the river morphology is relatively simple (e.g. alternating bars). In case of more complex morphologies, the use of a 2D model is recommended. For the 2D case, the prediction accuracy for the vertical dewatering rate and wetted area improved with higher spatial resolution; nevertheless the coarsest spatial resolution (maximum element area of 50 m^2) still provided satisfactory results with relative errors below 25%.

Our results indicate that the 1D models are not suitable for prediction of habitat suitability, even with high spatial resolutions. We found that weighted usable areas (WUA) derived from 1D model results differ substantially from WUA derived from the finest resolved 2D models, with relative deviations mostly larger than 50%, mainly due to differences in simulated flow velocities. We recommend the use of a highly resolved 2D model with spatial resolutions characterized by maximum element area between 1 m^2 and 10 m^2, since the use of coarser resolved 2D models also resulted in relative deviations larger than 25%.

Further, our results show how bed shear stress quantification is extremely sensitive to mesh resolution. For studies concerning macroinvertebrate drift, a 2D model with high spatial resolution with maximum element area in the order of ~1 m^2 or finer is thus recommended. Further investigations on the convergence of simulated bed shear stresses for resolutions with maximum element areas smaller than ~1 m^2 are necessary for an improved trade-off between accuracy and computational costs.

We also quantified the trade-offs between accuracy and computational efficiency: low spatial resolution 2D models show comparable speedup to the finest resolved 1D models, while generally obtaining more accurate results.

This systematic comparison of 1D and 2D hydrodynamic models with varying spatial resolution and river morphologies may be a useful guideline for modelers and planners to select an appropriate modelling approach for hydropeaking impact assessment. Beyond the considerations on the computational costs, the appropriate model choice should be driven by the ecohydraulic process of interest and the hydro-morphological characteristics of the studied reach.

Acknowledgments

The authors would like to thank Timo Wicki for his supporting work in this study in the frame of a Project Thesis at ETH Zurich.

References

[1] Auer, S., Zeiringer, B., Führer, S., Tonolla, D., and Schmutz, S. (2017). Effects of river bank heterogeneity and time of day on drift and stranding of juvenile european grayling (thymallus thymallus l.) caused by hydropeaking. *Science of the Total Environment*, 575:1515–1521.

[2] Baumann, P., Kirchhofer, A., and Schälchli, U. (2012). Sanierung schwall/sunk – strategische planung. Ein Modul der Vollzugshilfe Renatu-rierung der Gewässer. Bundesamt für Umwelt.

[3] Bejarano, M. D., Jansson, R., and Nilsson, C. (2018). The effects of hydropeaking on riverine plants: a review. *Biological Reviews*, 93(1):658–673.

[4] Benjankar, R., Tonina, D., and McKean, J. (2015). One-dimensional and two-dimensional hydrodynamic modeling derived flow properties: impacts on aquatic habitat quality predictions. *Earth Surface Processes and Landforms*, 40(3):340–356.

[5] Boavida, I., Santos, J. M., Ferreira, T., and Pinheiro, A. (2015). Barbel habitat alterations due to hydropeaking. *Journal of Hydro-environment Research*, 9(2):237–247.

[6] Bovee, K. D., Lamb, B. L., Bartholow, J. M., Stalnaker, C. B., and Taylor, J. (1998). Stream habitat analysis using the instream flow incremental methodology. Technical report.

[7] Brandt, S. A. (2000). Classification of geomorphological effects downstream of dams. *Catena*, 40(4):375–401.

[8] Brown, R. A. and Pasternack, G. B. (2009). Comparison of methods for analysing salmon habitat rehabilitation designs for regulated rivers. *River Research and Applications*, 25(6):745–772.

[9] Bruder, A., Tonolla, D., Schweizer, S. P., Vollenweider, S., Langhans, S. D., and Wüest, A. (2016). A conceptual framework for hydropeaking mitigation. *Science of the Total Environment*, 568:1204–1212.

[10] Bruno, M. C., Maiolini, B., Carolli, M., and Silveri, L. (2010). Short time-scale impacts of hydropeaking on benthic invertebrates in an alpine stream (trentino, italy). *Limnologica*, 40(4):281–290.

[11] Bruno, M. C., Siviglia, A., Carolli, M., and Maiolini, B. (2013). Multiple drift responses of benthic invertebrates to interacting hydropeaking and thermopeaking waves. *Ecohydrology*, 6(4):511–522.

[12] Casas-Mulet, R., Saltveit, S. J., and Alfredsen, K. (2015). The survival of atlantic salmon (salmo salar) eggs during dewatering in a river subjected to hydropeaking. *River Research and Applications*, 31(4):433–446.

[13] Fuller, I. C., Large, A. R., and Milan, D. J. (2003). Quantifying channel development and sediment transfer following chute cutoff in a wandering gravel-bed river. *Geomorphology*, 54(3-4):307–323.

[14] García, A., Jorde, K., Habit, E., Caamaño, D., and Parra, O. (2011). Downstream environmental effects of dam operations: changes in habitat quality for native fish species. *River Research and Applications*, 27(3):312–327.

[15] Garcia Lugo, G., Bertoldi, W., Henshaw, A., and Gurnell, A. (2015). The effect of lateral confinement on gravel bed river morphology. *Water Resources Research*, 51(9):7145–7158.

[16] García-Navarro, P., Murillo, J., Fernández-Pato, J., Echeverribar, I., and Morales-Hernández, M. (2019). The shallow water equations and their application to realistic cases. *Environmental Fluid Mechanics*, 19(5):1235–1252.

[17] Ghamry, H. and Katopodis, C. (2017). Computational optimization in simulating velocities and water-surface elevations for habitat–flow functions in low-slope rivers. *Journal of Ecohydraulics*, 2(2):99–121.

[18] Gibbins, C., Vericat, D., and Batalla, R. J. (2007). When is stream invertebrate drift catastrophic? the role of hydraulics and sediment transport in initiating drift during flood events. *Freshwater Biology*, 52(12):2369–2384.

[19] Gibson, S. A. and Pasternack, G. B. (2016). Selecting between one-dimensional and two-dimensional hydrodynamic models for ecohydraulic analysis. *River Research and Applications*, 32(6):1365–1381.

[20] Halleraker, J., Saltveit, S., Harby, A., Arnekleiv, J., Fjeldstad, H.-P., and Kohler, B. (2003). Factors influencing stranding of wild juvenile brown trout (salmo trutta) during rapid and frequent flow decreases in an artificial stream. *River Research and Applications*, 19(5-6):589–603.

[21] Harby, A., Alfredsen, K., Fjeldstad, H., Halleraker, J., Arnekleiv, J., Borsányi, P., Flodmark, L., Saltveit, S., Johansen,

S., Vehanen, T., et al. (2001). Ecological impacts of hydro peaking in rivers. In *Hydropower in the New Millennium*, pages 249–256. CRC Press.

[22] Harby, A., Sauterleute, J., Korpås, M., Killingtveit, Å., Solvang, E., and Nielsen, T. (2013). Pumped storage hydropower. In Stolten, D. and Scherer, V., editors, *Transition to renewable energy systems*, chapter 29, pages 597–618. Wiley.

[23] Hauer, C., Holzapfel, P., Leitner, P., and Graf, W. (2017). Longitudinal assessment of hydropeaking impacts on various scales for an improved process understanding and the design of mitigation measures. *Science of the Total Environment*, 575:1503–1514.

[24] Hauer, C., Schober, B., and Habersack, H. (2013). Impact analysis of river morphology and roughness variability on hydropeaking based on numerical modelling. *Hydrological Processes*, 27(15):2209–2224.

[25] Hauer, C., Unfer, G., Graf, W., Leitner, P., Zeiringer, B., and Habersack, H. (2012). Hydro-morphologically related variance in benthic drift and its importance for numerical habitat modelling. *Hydrobiologia*, 683(1):83–108.

[26] Hauer, C., Unfer, G., Holzapfel, P., Haimann, M., and Habersack, H. (2014). Impact of channel bar form and grain size variability on estimated stranding risk of juvenile brown trout during hydropeaking. *Earth Surface Processes and Landforms*, 39(12):1622–1641.

[27] Horritt, M., Bates, P., and Mattinson, M. (2006). Effects of mesh resolution and topographic representation in 2d finite volume models of shallow water fluvial flow. *Journal of Hydrology*, 329(1-2):306–314.

[28] Juárez, A., Adeva-Bustos, A., Alfredsen, K., and Dønnum, B. O. (2019). Performance of a two-dimensional hydraulic model for the evaluation of stranding areas and characterization of rapid fluctuations in hydropeaking rivers. *Water*, 11(2):201.

[29] Killingtveit, Å. (2013). Pumped storage hydropower. In Stolten, D. and Scherer, V., editors, *Transition to renewable energy systems*, chapter 20, pages 381–401. Wiley.

[30] Kjærstad, G., Arnekleiv, J. V., Speed, J. D. M., and Herland, A. K. (2018). Effects of hydropeaking on benthic invertebrate community composition in two central norwegian rivers. *River Research and Applications*, 34(3):218–231.

[31] Larrieu, K. G. and Pasternack, G. B. (2021). Automated analysis of lateral river connectivity and fish stranding risks. part 2: Juvenile chinook salmon stranding at a river rehabilitation site. *Ecohydrology*, page e2303.

[32] Larrieu, K. G., Pasternack, G. B., and Schwindt, S. (2021). Automated analysis of lateral river connectivity and fish stranding risks—part 1: Review, theory and algorithm. *Ecohydrology*, 14(2):e2268.

[33] Legleiter, C. J., Kyriakidis, P. C., McDonald, R. R., and Nelson, J. M. (2011). Effects of uncertain topographic input data on two-dimensional flow modeling in a gravel-bed river. *Water Resources Research*, 47(3).

[34] Leitner, P., Hauer, C., and Graf, W. (2017). Habitat use and tolerance levels of macroinvertebrates concerning hydraulic stress in hydropeaking rivers–a case study at the ziller river in austria. *Science of The Total Environment*, 575:112–118.

[35] Meile, T., Boillat, J.-L., and Schleiss, A. (2011). Hydropeaking indicators for characterization of the upper-rhone river in switzerland. *Aquatic Sciences*, 73(1):171–182.

[36] Moog, O. (1993). Quantification of daily peak hydropower effects on aquatic fauna and management to minimize environmental impacts. *Regulated Rivers: Research & Management*, 8(1-2):5–14.

[37] Nagrodski, A., Raby, G. D., Hasler, C. T., Taylor, M. K., and Cooke, S. J. (2012). Fish stranding in freshwater systems: sources, consequences, and mitigation. *Journal of environmental management*, 103:133–141.

[38] Noack, M., Schneider, M., and Wieprecht, S. (2013). The habitat modelling system casimir: a multivariate fuzzy-approach and its applications. In Maddock, I., Harby, A., Kemp, P., and Wood, P. J., editors, *Ecohydraulics: an integrated approach*, chapter 4, pages 75–89. John Wiley & Sons.

[39] Papaioannou, G., Papadaki, C., and Dimitriou, E. (2020). Sensitivity of habitat hydraulic model outputs to dtm and computational mesh resolution. *Ecohydrology*, 13(2):e2182.

[40] Papanicolaou, A., Elhakeem, M., and Wardman, B. (2011). Calibration and verification of a 2d hydrodynamic model for simulating flow around emergent bendway weir structures. *Journal of Hydraulic Engineering*, 137(1):75–89.

[41] Pasternack, G. B., Gilbert, A. T., Wheaton, J. M., and Buckland, E. M. (2006). Error propagation for velocity and shear stress prediction using 2d models for environmental management. *Journal of Hydrology*, 328(1-2):227–241.

[42] Pasternack, G. B., Wang, C. L., and Merz, J. E. (2004). Application of a 2d hydrodynamic model to design of reach-scale spawning gravel replenishment on the mokelumne river, california. *River Research and Applications*, 20(2):205–225.

[43] Person, E. (2013). *Impact of hydropeaking on fish and their habitat*. PhD thesis.

[44] Pisaturo, G. R., Righetti, M., Dumbser, M., Noack, M., Schneider, M., and Cavedon, V. (2017). The role of 3d-hydraulics in habitat modelling of hydropeaking events. *Science of the Total Environment*, 575:219–230.

[45] Saltveit, S., Halleraker, J., Arnekleiv, J., and Harby, A. (2001). Field experiments on stranding in juvenile atlantic salmon (salmo salar) and brown trout (salmo trutta) during rapid flow decreases caused by hydropeaking. *Regulated Rivers: Research & Management: An International Journal Devoted to River Research and Management*, 17(4-5):609–622.

[46] Tonina, D. and Jorde, K. (2013). Hydraulic modeling approaches for ecohydraulic studies: 3d, 2d, 1d and non-numerical models. In Maddock, I., Harby, A., Kemp, P., and Wood, P. J., editors, *Ecohydraulics: an integrated approach*, chapter 3, pages 31–74. John Wiley & Sons.

[47] Tonolla, D., Chaix, O., Meile, T., Zurwerra, A., Büsser, P., Oppliger, S., and Essyad, K. (2017). Schwall-sunk–massnahmen: ein modul der vollzugshilfe renaturierung der gewässer (in german).

[48] Toro, E. F. (2001). *Shock-capturing methods for free-surface shallow flows*. Wiley-Blackwell.

[49] Tuhtan, J. A., Noack, M., and Wieprecht, S. (2012). Estimating stranding risk due to hydropeaking for juvenile european grayling considering river morphology. *KSCE Journal of Civil Engineering*, 16(2):197–206.

[50] van Rooijen, E., Vanzo, D., Vetsch, D. F., Boes, R. M., and Siviglia, A. (2021). Enhancing an unsupervised clustering algorithm with a spatial contiguity constraint for river habitat analysis. *Ecohydrology*, page e2285.

[51] Vanzo, D., Peter, S., Vonwiller, L., Bürgler, M., Weberndorfer, M., Siviglia, A., Conde, D., and Vetsch, D. F. (2021). Basement v3: a modular freeware for river process modelling over multiple computational backends. *Environmental Modelling & Software*, page 105102.

[52] Vanzo, D., Zolezzi, G., and Siviglia, A. (2016). Eco-hydraulic modelling of the interactions between hydropeaking and river morphology. *Ecohydrology*, 9(3):421–437.

[53] Vetsch, D., Siviglia, A., Ehrbar, D., Facchini, M., Kammerer, S., Koch, A., Peter, S., Vanzo, D., Vonwiller, L., Gerber, M., Volz, C., Farshi, D., Mueller, R., Rousselot, P., Veprek, R., and Faeh, R. (2006–2017a). BASEMENT — Basic Simulation Environment for Computation of Environmental Flow and Natural Hazard Simulation, Version 2.7. ETH Zurich, VAW. http://www.basement.ethz.ch.

[54] Vetsch, D., Siviglia, A., Ehrbar, D., Facchini, M., Kammerer, S., Koch, A., Peter, S., Vonwiller, L., Gerber, M., Volz, C., Farshi, D., Mueller, R., Rousselot, P., Veprek, R., and Faeh, R. (2017b). *System Manuals of BASEMENT, Version 2.7. Laboratory of Hydraulics, Glaciology and Hydrology (VAW). ETH Zurich.* Available from http://www.basement.ethz.ch. [13.05.2021].

Conflicts of interest

The Authors declare that there are no conflicts of interest.

Data Availability Statement

The data that support the findings of this study are available from the corresponding author upon reasonable request.

List of Figures